How to cite: *Angew. Chem. Int. Ed.* **2025**, *64*, e202417217
doi.org/10.1002/anie.202417217

Rare Earth Metal Complexes

Stabilization of the Compressed Planar Benzene Dianion in Inverse-Sandwich Rare Earth Metal Complexes

*Francis Delano IV and Selvan Demir**

Abstract: For the first time, the capture of the planar antiaromatic parent benzene dianion in between two trivalent rare earth (RE) metal cations (RE^{III}), each stabilized by two guanidinate ligands, is reported. The synthesized inverse-sandwich complexes $[\{(Me_3Si)_2NC(N^iPr)_2\}_2RE]_2(\mu\text{-}\eta^6\text{:}\eta^6\text{-}C_6H_6)$, (RE = Y (**1**), Dy (**2**), and Er (**3**)) were crystallized from aprotic solvents and feature a remarkably planar parent benzene dianion, previously not encountered for any metal ion prone to low or absent covalency. The −2 charge localization at the benzene ligand was deduced from the results obtained by single-crystal X-ray diffraction analyses, spectroscopy, magnetometry, and Density Functional Theory (DFT) calculations. In the ^{1}H NMR spectrum of the diamagnetic Y complex **1**, the equivalent proton resonance of the bridging benzene dianion ligand is drastically shifted to higher field in comparison to free benzene. This and the calculated highly positive Nucleus-Independent Chemical Shift (NICS) values are attributed to the antiaromatic character of the benzene dianion ligand. The crucial role of the ancillary guanidinate ligand scaffold in stabilizing the planar benzene dianion conformation was also elucidated by DFT calculations. Remarkably, the planarity of the benzene dianion originates from the stabilization of the π-type orbitals of the d-manifold and compression through its strong electrostatic interaction with the two RE^{III} sites.

Introduction

Aromaticity is a core principle in chemistry with extensive applications resulting in a significant body of research devoted to developing a deeper understanding of this property. Accordingly, approximately two-thirds of all known molecules are aromatic or consist of aromatic rings.[1]

[*] F. Delano IV, Prof. Dr. S. Demir
Department of Chemistry
Michigan State University
578 South Shaw Lane, East Lansing, Michigan, 48824, USA
E-mail: sdemir@chemistry.msu.edu

The archetypal example of an aromatic compound is benzene whose highly delocalized electronic structure, enhanced thermodynamic stability, and bond length equalization has been an area of intrigue since Kekulé's dream of a snake biting its own tail.[2] The seminal formalism of predicting the aromaticity of a system was provided by Hückel suggesting that planar π-systems are stabilized (aromatic) when they possess $4n+2$ π-electrons and destabilized (antiaromatic) when they possess $4n$ π-electrons.[3] Since then, the concept of aromaticity has been expanded to describe systems with enhanced stability, including organometallic-,[4] metal-,[5,6] and semimetal-clusters.[7]

Notably, sandwiching benzene between two electropositive metals in an anti-coordination mode, stabilizes various formal charges of the π-system spanning from 0 (6π-electrons), −2 (8π-electrons) to −4 (10π-electrons); Figure 1.[8–11] Since the discovery of an inverse-sandwich complex in 1983 (Figure 1, left, top),[12] complexes of this class have garnered a great deal of interest due to their unique electronic characteristics and bonding. The symmetric match of the highest occupied molecular orbitals of the reduced species and the metal-based d-orbitals result in the generation of both π and δ interactions. However, the differing degrees in metal-arene covalency and charge delocalization allow for numerous metal–arene charge combinations, rendering an assignment of the formal oxidation states in complexes with bridging arene units difficult.[13]

Innate to an aromatic compound, planar geometries maximize the overlap of the atomic p-orbitals of the π-system. This interaction is highly stabilizing for aromatic systems but highly destabilizing to antiaromatic systems.[14] Hence, deviations from planarity frequently occur for arene compounds with additional electronic charges to accommodate the surplus of negative charge residing on the arene. The resulting expansion of the arene ring, and ring puckering has been attributed to partial occupation of the arene's π* molecular orbitals combined with both first and second order Jahn–Teller distortions. Herein, we report the first isolation of a planar parent benzene dianion with any s-, p-, d-, or 4f- metals, which is stabilized by two rare earth (RE) metal centers adopting an anti-conformation with respect to the bridging ring.

Results and Discussion

The first guanidinate benzene-bridged RE metal complexes $[\{(Me_3Si)_2NC(N^iPr)_2\}_2RE]_2(\mu\text{-}\eta^6\text{:}\eta^6\text{-}C_6H_6)$ (RE = Y (**1**), Dy (**2**), and Er (**3**)) were synthesized through the chemical

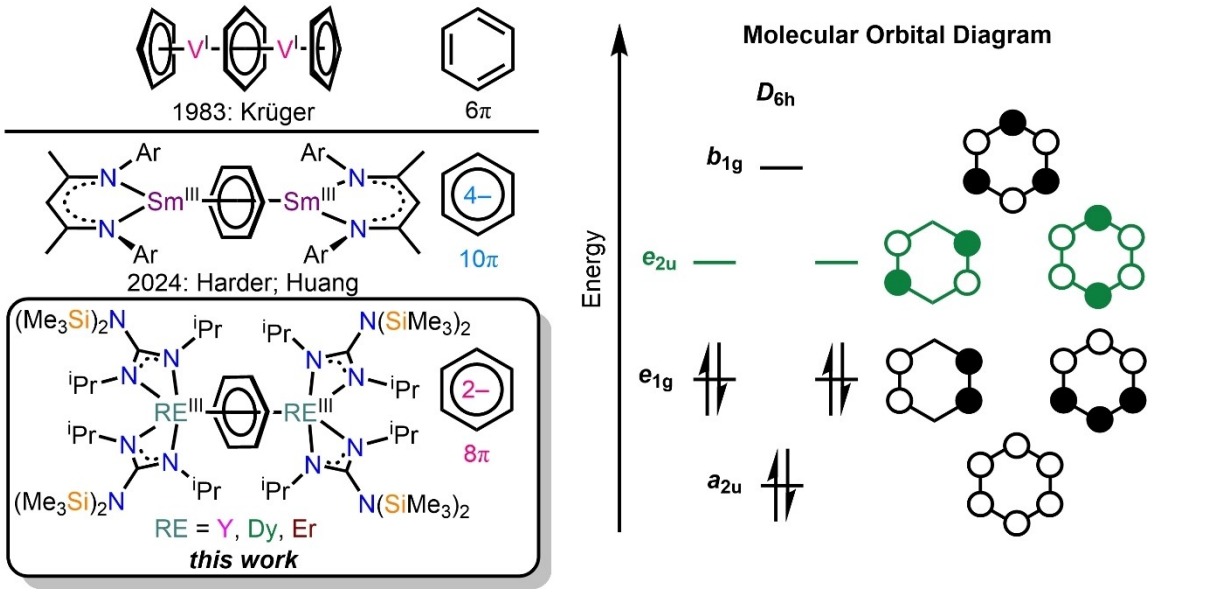

Figure 1. (left) Examples of inverse-sandwich complexes bearing various charged parent benzene units. (right) Molecular orbital diagram of benzene. The orbitals highlighted in green are the lowest unoccupied molecular orbitals (LUMOs). The corresponding reduced π ligand can participate in π or δ interactions with metal-based *d* orbitals, owing to the good match in orbital symmetry.

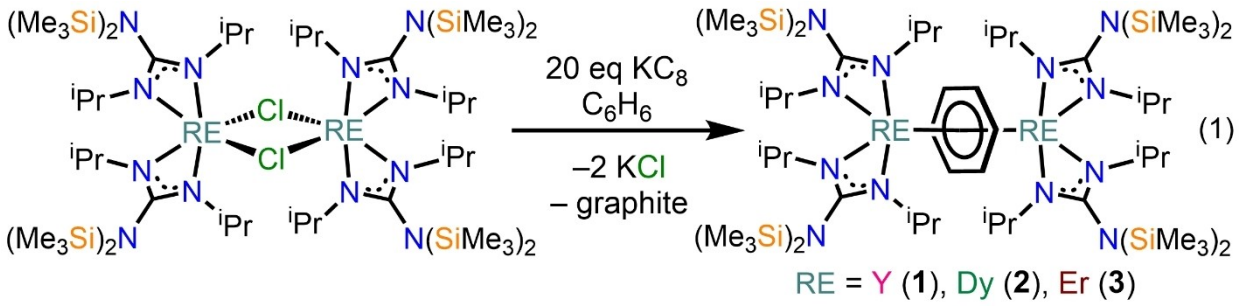

reduction of the parent halide-bridged complexes $[\{(Me_3Si)_2NC(N^iPr)_2\}_2RE(\mu\text{-}Cl)]_2$ with 20 molar equiv. of KC_8 in benzene over the course of 12 hours (eq. 1, Figure 2). After removal of insoluble material, the resulting red colored solutions were evaporated to dryness to give red and orange solids which were extracted with *n*-hexane. Yellow, red, and orange crystals suitable for single-crystal X-ray diffraction analysis of **1**, **2**, and **3** were grown from concentrated *n*-hexane solution at −35 °C in 24, 20, and 26 % crystalline yields, respectively.

Typical of an inverse-sandwich complex, the molecular geometry introduces several possibilities regarding the delocalization of charge: 1) two trivalent rare earth ions and a bridging $(C_6H_6)^{2-}$ unit; 2) two divalent rare earth ions and a neutral arene unit; 3) A mixed-valent complex with either one divalent and one trivalent RE ion or two RE ions with a formally assigned 2.5 oxidation state, where in either case the metal centers are bridged by a benzene monoanion. In general, inverse-sandwich complexes with anionic bridging arenes feature considerable torsion of the central arene unit (*Supporting Information*, Table S1). The highly Lewis acidic lanthanide ions can also interact with the face of neutral arenes in a η^6-fashion.[15] One proposed mechanism for the formation of complexes of this class traverses through direct metal-metal bonds, emerged from reductions of halide-containing complexes.[16,17] Recently, a similar synthetic route led to molecules composed of tetraanionic bridging benzene units.[8–10] Bulky guanidinate ligands provide sufficient stabilization of metal cations to foster the generation of metal-metal bonds with metals in low, hence, reactive oxidation states under reductive reaction conditions.[18]

The sterically cumbersome nature of such ancillary ligand scaffolds protects metals from coordination to solvent molecules, yet the metal-metal bond activates small molecules through electron transfer.[18,19] Guanidinate ligands attached to RE ions have yielded complexes that are either relevant for single-molecule magnetism,[20–22] or viable to construct multimetallic compounds with bridging redox-active ligands.[23,24] In addition, amidinate anions that are electronically and structurally similar to guanidinates are able to stabilize the highly reactive divalent oxidation state of both Tb and Dy.[25]

As the ionic radii of Y, Dy, and Er are quite similar (Y = 1.019 Å, Dy = 1.027 Å, and Er = 1.004 Å, CN = 8)[26] and the

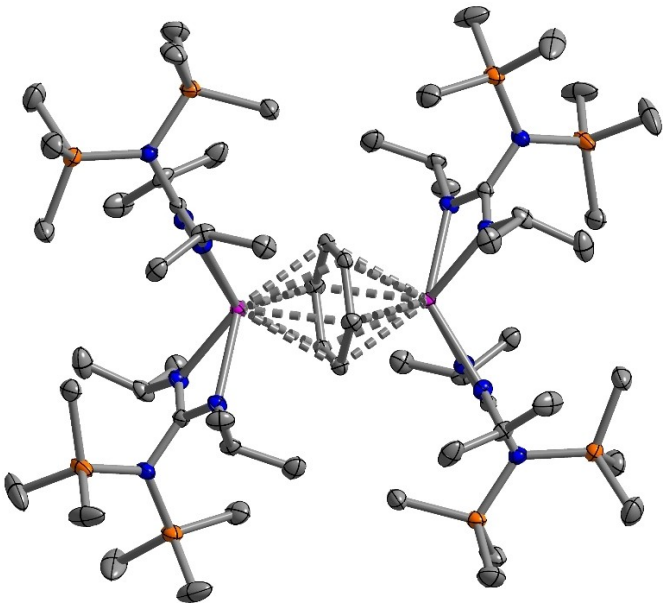

Figure 2. Structure of $[\{(Me_3Si)_2NC(N^iPr)_2\}_2Y]_2(\mu\text{-}\eta^6\text{:}\eta^6\text{-}C_6H_6)$, **1**, in a crystal of $[\{(Me_3Si)_2NC(N^iPr)_2\}_2Y]_2((\mu\text{-}\eta^6\text{:}\eta^6\text{-}C_6H_6)\cdot C_6H_{14}$ with thermal ellipsoids drawn at the 50% probability level. Pink, orange, blue, and gray ellipsoids represent Y, Si, N, and C atoms, respectively. Hydrogen atoms have been omitted for clarity. The structures of **2** and **3** are shown in Figures S6–S9. Selected interatomic distances (Å) and angles (°): Y–N_{guan} = 2.340(2)–2.429(2); Y–C_{Arene} = 2.662(2)–2.702(2); Y···Y = 4.515(1); C_{guan}–Y–C_{guan} = 121.0(6); Dy–N_{guan} = 2.324(1)–2.478(1); Dy–C_{Arene} = 2.685(3)–2.711(3); Dy···Dy = 4.569(1); C_{guan}–Dy–C_{guan} = 120.3(7); Er–N_{guan} = 2.338(1)–2.420(1); Er–C_{Arene} = 2.645(7)–2.689(6); Er···Er = 4.513(1); C_{guan}–Er–C_{guan} = 121.5(2).

topology of the structure is nearly identical, one would expect similar unit cells. However, the three complexes crystallize in different unit cells (*Supporting Information*, Table S3). In all cases, the primary coordination sphere of each metal center comprises two bidentate guanidinate anions and the face of the bridging $(C_6H_6)^{2-}$ unit binds in an η^6-fashion. Fascinatingly, the bridging benzene unit remains completely planar (Figures 2 and S11).

In all cases, the intermetallic RE···RE distances of 4.515(1) Å (Y, **1**), 4.569(1) Å (Dy, **2**), and 4.513(1) Å (Er, **3**) exceed the sum of the ionic radii of the two metal centers $(\Sigma\{RE^{III}\}_2$ (each RE CN = 8): 2.038 Å (Y), 2.054 Å (Dy), and 2.008 Å (Er)). The guanidinate anions coordinate asymmetrically to the metal centers with RE–N_{guan} distances ranging from 2.340(2)–2.429(2) Å, 2.324(1)–2.478(1) Å, and 2.338(1)–2.420(1) Å, for **1**, **2**, and **3**, respectively. In all cases, the range of these interatomic distances is slightly larger than those observed for the parental halide-bridged complexes $[\{(Me_3Si)_2NC(N^iPr)_2\}_2RE(\mu\text{-}Cl)]_2$ (RE = Y: 2.326(4)–2.388(4) Å, RE = Dy: 2.334(4)–2.422(4) Å, and RE = Er: 2.300(2)–2.409(1) Å.[20,24] The comparable RE–N_{guan} interatomic distances are suggestive of trivalent RE metal cations as a divalent oxidation state typically corresponds to an increase in ionic radius of nearly 0.1 Å.[27]

The interatomic RE–C_{arene} distances are inequivalent and span from 2.662(2) to 2.702(2) Å, from 2.685(3) to 2.711(3) Å, and from 2.645(7) to 2.689(6) Å in **1**, **2**, and **3**, respectively. These distances are shorter than the La–C_{arene} interatomic distances of 2.75(1)–2.79(1) Å found in $[K(18\text{-}c\text{-}6)][(Cp^{tt}{}_2La)_2(\mu\text{-}\eta^6\text{:}\eta^6\text{-}C_6H_6)]$ (18-c-6 = 18-crown-6; $Cp^{tt} = C_5H_3(CMe_3)_2$), which is composed of divalent La ions and a $(C_6H_6)^-$ bridging monoanion, Figure S2.[28] Hence, the discrepancy in interatomic distances may be attributed to the difference in ionic sizes and oxidation states.

The charge of the bridging arene within inverse-sandwich complexes may be interpreted through scrutinizing the interatomic C–C distances. The successive population of the formally π* (e_{2u}) orbitals results in an substantial elongation due to an increased antibonding character.[29] In the singlet ground state, the interatomic C–C distances are inequivalent, corresponding to a compressed cyclohexadienediide electronic structure. By contrast, in the triplet state, the C–C distance remain equivalent, and the benzene unit adopts a D_{6h} geometry. Typically, the compressed cyclohexadienediide electronic structure corresponds to significant ring puckering resulting in a pseudo C_{2v} boat conformation. In the case of **1**, **2**, and **3**, the interatomic C–C distances are inequivalent and engender two categorically different groups (Figure S11) consistent with the description of a quinoidal structure displaying two short (1.373(3) Å (**1**); 1.375(4) Å (**2**) and 1.358(8) Å (**3**)) and four long C–C bonds (1.451(1)–1.490(3) Å; 1.430(4)–1.496(4) Å; and 1.437(9)–1.478(10) Å for **1**, **2**, and **3**, respectively). Overall, a significant geometric distortion arises relative to free benzene (av. C–C = 1.397(9) Å),[30] suggestive of negative charges residing at the *para*-positions which is typical of a cyclohexadienediide-type electronic structure.[29] Two of the endocyclic C–C–C angles of 117.2(2), 118.4(2), and 117.8(5)° for **1**, **2**, and **3**, respectively, are identical and slightly narrower relative to the four other identical angles (121.4(2)° (**1**); 120.8(8)° (**2**); and 121.1(8)° (**3**)). Notably, mononuclear complexes of La, Ce, Pr, and Nd containing a cyclohexadienediide dianion feature a boat confirmation of the bridging arene ring, and a $\kappa^2\text{:}\eta^1,\eta^1$ coordination mode.[31] A similar cyclohexadienediide-type electronic structure occurs in $[(^{DIPeP}BDI)Sr]_2(C_6H_6)$ ($^{DIPeP}BDI$ = HC[C(Me)N-(2,6-$CH(Et)_2$-phenyl)]$_2$, albeit substantially more distorted.[32] In general, the emergence of a $(C_6H_6)^{2-}$ moiety impacts the C–C–C–C torsion angle considerably (see Table S2) leading to a nonplanar bridge. Remarkably, the bridging unit for **1**, **2**, and **3** remains completely planar. Notably, the only occurrence of planar dianionic parent benzene bridges is when paired with uranium which emergence is rationalized through the greater covalency enabled by the 5f-orbitals allowing stabilization through δ-backbonding (Table S3).[33,34] Such δ-backbonding is impossible for the contracted 4f orbitals, rendering the results on hand intriguing. As Y^{III} is innate to limited expandable d-orbitals and lacks f-orbitals, we sought to probe its ability to engage in covalent bonding through Density Functional Theory (DFT) methods.

The d^0 electron configuration of the Y^{III} ion simplifies the investigation of both the bonding situation and electronic structure through DFT. Because of the large computational cost associated with the rotation of the ancillary

trimethylsilyl groups, a simplified structure of **1** was considered where the $SiMe_3$ groups of the guanidinate ligand were replaced by CH_3. Owing to the ambiguity of the spin-state of the bridging benzene unit, two different spin multiplicities were considered when performing geometry optimizations. The geometry of the resulting complex, $[\{Me_2NC(N^iPr)_2\}_2Y]_2(\mu\text{-}\eta^6\text{:}\eta^6\text{-}C_6H_6)$, henceforth referred to as **1′**, was optimized as both an open–shell triplet and singlet employing six different functionals. Further computational details are provided in the *Supporting Information*. Comparison of the optimized coordinates with the crystallographically determined structure reveals that the hybrid exchange–correlated functional uCAMB3LYP[35] and singlet multiplicity best reproduced the experimental results (Tables S6–S10). The highest occupied molecular orbital (HOMO) is best described as a δ bond between each metal centered 4d orbital and the π*-orbital of the bridging benzene moiety. The lowest unoccupied molecular orbital (LUMO) comprises the π-orbitals of the bridging benzene unit and d orbitals of the metal (Figure 3). **1′** was investigated through a natural localized molecular orbital (NLMO)[36,37] analysis, to provide insight into the bonding situation between the arene–bridge and metal ions (Table S12). The interactions are found within the second–order perturbation analysis, indicative of an ionic bonding situation. The strongest interactions (24.72 and 24.45 kcal mol^{-1}) stem from donations arising from the p orbital-centered lone pairs of the nucleophilic carbons into the yttrium–based lone valencies, consistent with the compressed cyclohexadienediide conformation of the dianionic benzene ring. Smaller, but still significant stabilization energies (1.26–11.65 kcal mol^{-1}) are additionally observed from donations originating from the C–C σ- and π-bonds. The localization of the anionic charges can also be monitored through the calculated charge at each of the carbon atoms of the benzene ligand.

To probe the aromaticity of the bridging benzene unit, Nucleus–Independent Chemical Shift (NICS) calculations were performed. Negative NICS values are indicative of aromaticity, whereas positive values suggest antiaromaticity. Calculations of this type have been carried out on similar complexes including $[Gd_2(BzN_6\text{–}Mes)]^{2-}$ where the 1,3,5-tris[2′,6′-(*N*-mesityl)dimethanamino-4′-*tert*-butylphenyl]benzene (BzN_6–Mes) bridging unit exhibits Baird aromaticity.[38] The magnetic shielding tensors were calculated at the geometric center as well as the axis perpendicular to the ring plane of the bridging benzene unit. The NICS(0) value of 50.35 ppm (Figure 4) calculated at the center of the anion benzene unit implies antiaromatic character,[39] in accordance with the suspected cyclohexadienediide electronic structure.

The energy difference between the triplet and singlet spin states of benzene dianions is small and postulated to be thermally accessible.[16,32] A triplet spin state causes an equilibration of the interatomic C–C distances, corresponding to a Baird aromat.[19] To assess any structural transformations with elevated temperature, a variable-temperature single-crystal X-ray diffraction experiment was undertaken where the crystal structure of **1** was measured at temperatures spanning from 100 to 220 K (Figures S10 and S12). A scrutiny of all collected crystallographic information revealed insignificant alterations to the interatomic C–C distances, indicative of selective population of the singlet state over the entire probed temperature range.

Topologically similar RE metal complexes containing ligands such as cyclopentadienyl derivatives exhibit substantial ring strain engendering a nonplanar conformation of bridging arene anions. To assess the role of the ancillary ligand scaffold, the geometry of the hypothetical molecules $[(Cp'_2Y)_2(\mu\text{-}\eta^6\text{:}\eta^6\text{-}C_6H_6)]^{n-}$ ($Cp' = C_5H_4(SiMe_3)$; $n = 0$, 2) and

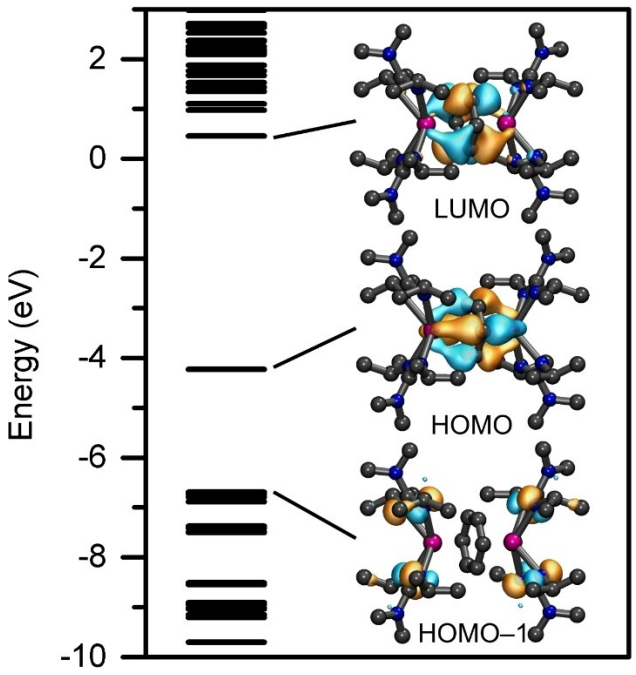

Figure 3. Calculated frontier orbitals of $[\{Me_2NC(N^iPr)_2\}_2Y]_2(\mu\text{-}\eta^6\text{:}\eta^6\text{-}C_6H_6)$, **1′**, with the uCAMB3LYP functional and def2-TZVP basis set. See *Supporting Information* for details. All isovalues were set to 0.4.

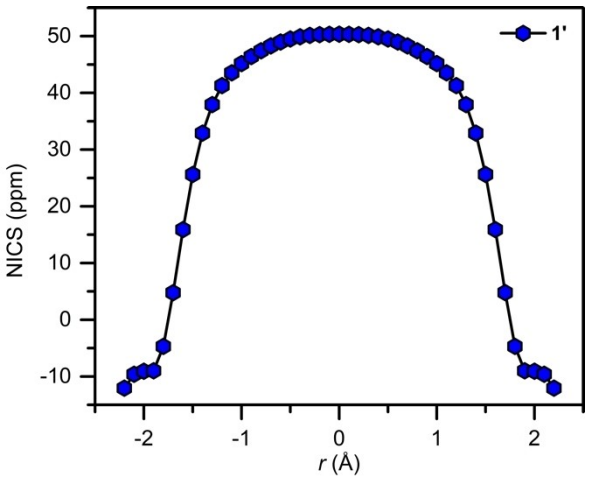

Figure 4. Plot of the NICS values for $[\{Me_2NC(N^iPr)_2\}_2Y]_2(\mu\text{-}\eta^6\text{:}\eta^6\text{-}C_6H_6)$, **1′**, measured ±2 Å from the centroid of the ring plane in the C_6H_6 moiety in 0.1 Å intervals.

$[(\{(Me_3Si)_2NC(N^iPr)_2\}_2Y)_2(\mu\text{-}\eta^6\text{:}\eta^6\text{-}C_6H_6)]^{n-}$ ($n=0$, 2, 4) were optimized as singlets, where the relevant computational details are provided in the *Supporting Information*. The predicted geometries of all molecules are depicted in Figure S37. The identity of the ancillary ligand plays a significant role in the observed planarity of the bridging benzene unit, largely owing to the relative energies of the Y d-manifold.

The d-orbital splitting pattern has also been used to rationalize the difference in electronic configuration of a series of divalent RE metal complexes.[40] Similarly to the tris-cyclopentadienyl series of Y complexes, which possesses a lowest energy d_z^2 orbital,[41] a lone valance of the metallocene motif in $[(Cp'_2Y)_2(\mu\text{-}\eta^6\text{:}\eta^6\text{-}C_6H_6)]$ is d_z^2 in character and resides perpendicular to the plane defined by the metal center and centroids of the cyclopentadienyl ring. Owing to the asymmetry of the complexes, the crystal field splitting of the Y centers in $[(Cp'_2Y)_2(\mu\text{-}\eta^6\text{:}\eta^6\text{-}C_6H_6)]$ are inequivalent and thus, have different electronic contributions. For one center, two metal-based orbitals of appropriate symmetry form a σ-type bonding interaction with lone pairs of the bridging arene (9.77 and 9.83 % Y). Notably, the crystal field splitting of the ancillary guanidinate anions only allows for ionic bonding interactions between the metal and bridging benzene unit, likely owing to the differing crystal field.

The electronic absorption spectra of **1**, **2**, and **3** closely resemble and exhibit three main absorption bands at 3.6×10^4 cm^{-1}, 3.1×10^4 cm^{-1}, and 2.4×10^4 cm^{-1} (Figure 5). The similarities of the spectra imply that the predominant transitions arise from the ancillary ligand scaffold. The identity of the calculated transitions is provided in Table S13. The lack of low energy transitions in the UV/Vis spectra further confirms the metal centers in **1**, **2**, and **3** to be trivalent cations, as the presence of such transitions are commonly attributed to the divalent oxidation state of the rare earth metals.[42,43] The ^{1}H NMR spectrum of **1** displays one resonance for the protons of the bridging benzene ligand at $\delta=1.67$ ppm, which is drastically shifted to higher field relative to free benzene ($\delta=7.12$ ppm, toluene-d_8)[44] (Figure S17). The higher shielding of the equivalent protons of the benzene ligand in **1** is attributed to the anionic charge and the paratropic ring current, in accordance with the antiaromatic character as suggested by the very positive NICS values (Figure 4).

The paramagnetic metal ions Dy^{III} and Er^{III} with substantially different electron density distribution are prone to give varying magnetic behavior when encased in the same coordination environment. To probe this, dc magnetic susceptibility data were collected from 2 to 300 K for **2** and **3** under 0.1, 0.5, and 1.0 T applied dc fields, respectively (Figures 6, S21, and S22). At 1.0 T, the room temperature $\chi_M T$ values of 28.54 $cm^3\,K\,mol^{-1}$ and 22.01 $cm^3\,K\,mol^{-1}$ for **2** and **3**, respectively, are in good agreement with the expected values of 28.24 $cm^3\,K\,mol^{-1}$ and 22.96 $cm^3\,K\,mol^{-1}$ for two noninteracting Dy^{III} and Er^{III} ions, respectively. A gradual downturn in $\chi_M T$ occurs as the temperature is lowered for both **2** and **3**, in accordance to the depopulation of the m_J sublevels,[45] and the absence of magnetic exchange coupling. At weaker applied fields and as temperature is lowered, a distinct rise in $\chi_M T$ is observed for **3** up to a maximum value of 35.52 $cm^3\,K\,mol^{-1}$ at 5.40 K (0.1 T). This suggests the presence of weak exchange coupling pathways between multiple Er^{III} centers, which are effectively diminished upon the application of higher magnetic fields. Owing to the differences in crystal packing of **2** and **3**, a direct comparison of interactions is not possible. However, the topological similarities between the series suggests this coupling scheme is ascribed to intermolecular dipolar coupling. This type of interaction can control the energy levels and transition probabilities of Er^{III}-based SMMs.[46,47] Notably, the closest inter- and intramolecular Er···Er distances are 9.470(1) and 4.506(1) Å, respectively. The reduced magnetization curves (M vs. H/T) are non-superimposable at temperatures

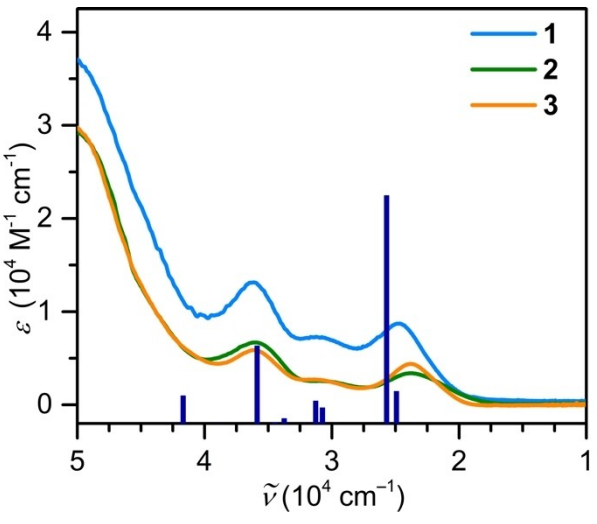

Figure 5. UV/Vis absorption spectra of $[\{(Me_3Si)_2NC(N^iPr)_2\}_2RE]_2(\mu\text{-}\eta^6\text{:}\eta^6\text{-}C_6H_6)$, (RE = Y (**1**), Dy (**2**), and Er (**3**)), taken in *n*-hexane solution. Light blue, green, and orange lines represent experimental data for **1**, **2**, and **3**, respectively, whereas dark blue vertical lines constitute calculated TDDFT transitions of $[\{Me_2NC(N^iPr)_2\}_2Y]_2((\mu\text{-}\eta^6\text{:}\eta^6\text{-}C_6H_6)$, **1′**.

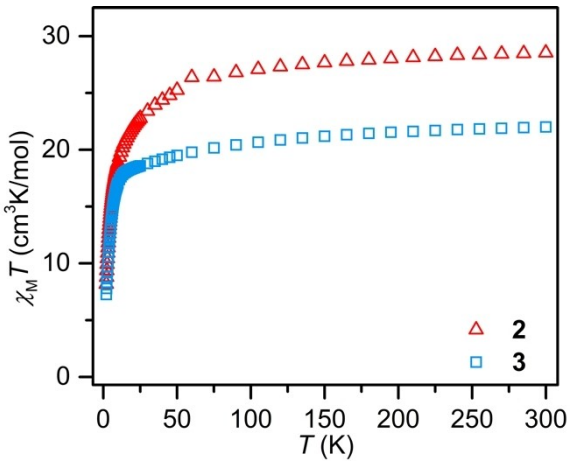

Figure 6. Variable-temperature dc magnetic susceptibility data for $[\{(Me_3Si)_2NC(N^iPr)_2\}_2RE]_2(\mu\text{-}\eta^6\text{:}\eta^6\text{-}C_6H_6)$, (RE = Dy (**2**), and Er (**3**)), collected under a 1.0 T applied dc field.

ranging from 2 to 10 K, attributable to significant magnetic anisotropy (Figures S32 and S34).

When paired with hard anionic donors that accentuate the innate single-ion anisotropy of the Dy^{III} and Er^{III} ions, such as guanidinate anions, single-molecule magnet (SMM) behavior can arise. SMMs are molecules which can retain their magnetization in the absence of a magnetic field.[48] Such molecules possess an intrinsic doubly degenerate ground state, and when paired with an appropriate crystal field, can exhibit slow magnetic relaxation.[49–52] For the construction of multinuclear SMMs innate to real magnetic memory as showcased by open magnetic hysteresis loops, strong magnetic exchange coupling is the most effective owing to a powerful suppression of fast relaxation pathways.[53] This is best achieved by metal-metal bonds or radical bridges in between metal ions.[54–57] Intriguingly, anionic arene bridges may engender strong magnetic communication or exchange coupling between metals,[38,58] which is less developed. To probe the presence of SMM behavior, the dynamic properties of **2** and **3** were explored. **2** displays signals in the out-of-phase (χ_M'') components of the magnetic susceptibility, however, the peak maximum lies past 1000 Hz therefore prevents the determination of relaxation times (Figure S23).

Fast magnetic relaxation pathways can be mitigated through the application of an external magnetic field. The magnitude of the optimal applied external magnetic field was determined by measuring the out-of-phase χ_M'' components of the ac magnetic susceptibility from 0 to 2250 Oe and 0 to 1500 Oe for **2** and **3**, respectively. The application of an external magnetic field was found to usher into the emergence of χ_M'' ac magnetic susceptibility signals. Under all fields investigated, the χ_M'' peak maximum of **2** remains past 1000 Hz, thus prohibiting the determination of relaxation times (Figure S25).

However, **3** displays χ_M'' signals under the application of a 750 Oe applied dc field from 1.8 to 2.4 K. Here, the extraction of the relaxation times proceeded from the fits of the Cole–Cole plots employing the program CCFit2,[59] Figure S29, which were subsequently fit to a generalized Debye model. A satisfactory fit of the experimentally determined relaxation times was achieved by considering an Orbach relaxation process: $ln(\tau) = ln(\tau_o) + \frac{U_{eff}}{k_B T}$. The best fit afforded fitting parameters of $U_{eff} = 14.0(3)$ cm^{-1} and $\tau_o = 9.6(1) \times 10^{-8}$ s. Albeit no benzene-bridged Er SMM is known for comparison, the obtained values are similar to the few other erbium-based SMMs featuring an inverse-sandwich molecular structure such as $[(NN^{TBS})Er]_2$(μ-biphenyl)[K(18-crown-6)]$_2$ [NN^{TBS} = 1,1′-Fc(NSi^tBuMe_2)$_2$] ($U_{eff} = 17.4$ cm^{-1}; $\tau_o = 4.7 \times 10^{-6}$ s).[60]

Conclusions

In conclusion, the peerless rare earth inverse-sandwich complexes $[\{(Me_3Si)_2NC(N^iPr)_2\}_2RE]_2(\mu\text{-}\eta^6\text{:}\eta^6\text{-}C_6H_6)$, (RE = Y (**1**), Dy (**2**), and Er (**3**)) with guanidinate scaffolds at the RE^{III} centers and a remarkably planar bridging benzene dianion ligand were isolated and unambiguously characterized. This is simultaneously the first report of a planar bridging parent benzene unit for any compound composed of s-, p-, d-, or 4f-metal ions. In these complexes, the formal −2 charge and antiaromatic character has been ascribed to the bridging benzene ligand based on bond length analysis, spectroscopy, SQUID magnetometry, and computations. The striking planarity of the benzene dianion originates from the stabilization of the π-type orbitals of the d-manifold and compression through its strong electrostatic interaction with the two RE^{III} sites. Interestingly, computational results suggest that the planarity of the parent benzene dianion cannot occur for classical organometallic ligand scaffolds such as ancillary cyclopentadienyl anions, further emphasizing a stronger stabilizing effect of guanidinate ligands to rare earth metal ions. The ongoing study has huge ramifications for the in situ access of highly reactive low-valent RE ion species stabilized by guanidinate scaffolds and their reactivity towards substrates. This may pave the way for unprecedented compounds innate to elusive types of reduced substrates beyond the benzene example in the future.

Supporting Information

The authors have cited additional references within the Supporting Information.[10,11,20,24,61–111] CCDC 2368983, 2368984, 2368985, 2368986, 2368987, 2368988, 2368989 (compound **1** measured at different temperatures), 2368981 (compound **2**), 2368982 (compound **3**), contain the supplementary crystallographic data for this paper. These data can be obtained free of charge via www.ccdc.cam.ac.uk/data_request/cif, or by emailing data_request@ccdc.cam.ac.uk, or by contacting The Cambridge Crystallographic Data Centre, 12 Union Road, Cambridge CB2 1EZ, UK; fax: +44 1223 336033.

Acknowledgements

This work was funded in part through the National Science Foundation (NSF) Faculty Early Career Development Program (CAREER) CHE-2339595. S.D. is grateful to the Department of Chemistry at Michigan State University (MSU) for generous start-up funds. We are grateful to Dr. Rui Huang and Dr. Richard Staples (MSU) for assistance with CHN and X-ray diffraction analyses, respectively. We thank Florian Benner for experimental assistance. This work was supported in part through computational resources and services provided by the Institute for Cyber-Enabled Research at MSU. Funding for the single-crystal X-ray diffractometer was provided through the MRI program by the National Science Foundation under Grant No. 1919565.

Conflict of Interest

The authors declare no conflict of interest.

Data Availability Statement

The data that support the findings of this study are available in the supplementary material of this article.

Keywords: Aromaticity · Lanthanides · Magnetism · Organometallic Complexes · SMM

[1] A. T. Balaban, D. C. Oniciu, A. R. Katritzky, *Chem. Rev.* **2004**, *104*, 2777–2812.
[2] A. Kekulé, *Bull. Soc. Chim. Fr.* **1865**, *3*, 98–110.
[3] E. Hückel, *Z. Phys.* **1931**, *70*, 204–286.
[4] J. T. Boronski, J. A. Seed, D. Hunger, A. W. Woodward, J. van Slageren, A. J. Wooles, L. S. Natrajan, N. Kaltsoyannis, S. T. Liddle, *Nature* **2021**, 1–7.
[5] X. Li, A. E. Kuznetsov, H.-F. Zhang, A. I. Boldyrev, L.-S. Wang, *Science* **2001**, *291*, 859–861.
[6] B. Peerless, A. Schmidt, Y. J. Franzke, S. Dehnen, *Nat. Chem.* **2023**, *15*, 347–356.
[7] V. Ya Lee, A. Sekiguchi, *Angew. Chem. Int. Ed.* **2007**, *46*, 6596–6620.
[8] Y. Wang, Y. Zhang, J. Liang, B. Tan, C. Deng, W. Huang, *Chem. Sci.* **2024**, *15*, 10669–10669.
[9] Y. Wang, Y. Zhang, J. Liang, B. Tan, C. Deng, W. Huang, *Chem. Sci.* **2024**, *15*, 8740–8749.
[10] S. K. Thakur, N. Roig, R. Monreal-Corona, J. Langer, M. Alonso, S. Harder, *Angew. Chem. Int. Ed.* **2024**, *63*, e202405229.
[11] W. Huang, F. Dulong, T. Wu, S. I. Khan, J. T. Miller, T. Cantat, P. L. Diaconescu, *Nat. Commun.* **2013**, *4*, 1448.
[12] A. W. Duff, K. Jonas, R. Goddard, H. J. Kraus, C. Krueger, *J. Am. Chem. Soc.* **1983**, *105*, 5479–5480.
[13] M. N. Bochkarev, *Chem. Rev.* **2002**, *102*, 2089–2118.
[14] B. L. Podlogar, W. A. Glauser, W. R. Rodriguez, D. J. Raber, *J. Org. Chem.* **1988**, *53*, 2127–2129.
[15] M. E. Hossain, Z. Guo, J. Wang, G. B. Deacon, P. C. Junk, D. Diether, R. Anwander, *Eur. J. Inorg. Chem.* **2022**, *2022*, e202101009.
[16] B. Rösch, T. X. Gentner, J. Langer, C. Färber, J. Eyselein, L. Zhao, C. Ding, G. Frenking, S. Harder, *Science* **2021**, *371*, 1125–1128.
[17] D. Jędrzkiewicz, J. Langer, S. Harder, *Z. Anorg. Allg. Chem.* n.d., *n/a*, e202200138.
[18] S. P. Green, C. Jones, A. Stasch, *Science* **2007**, *318*, 1754–1757.
[19] D. D. L. Jones, I. Douair, L. Maron, C. Jones, *Angew. Chem. Int. Ed.* **2021**, *60*, 7087–7092.
[20] P.-B. Jin, K.-X. Yu, Y.-Q. Zhai, Q.-C. Luo, Y.-D. Wang, X.-F. Zhang, Y. Lv, Y.-Z. Zheng, *Chin. J. Chem.* **2021**, *39*, 1635–1640.
[21] F. Delano IV, S. Demir, *Cryst. Growth Des.* **2023**, *23*, 3134–3143.
[22] F. Delano, S. Deshapriya, S. Demir, *Polyhedron* **2024**, *249*, 116785.
[23] F. Delano IV, S. Deshapriya, S. Demir, *Inorg. Chem.* **2024**, *63*, 9659–9669.
[24] F. Delano IV, S. Demir, *Eur. J. Inorg. Chem.* **2024**, *27*, e202300797.
[25] P.-B. Jin, Q.-C. Luo, G. K. Gransbury, I. J. Vitorica-Yrezabal, T. Hajdu, I. Strashnov, E. J. L. McInnes, R. E. P. Winpenny, N. F. Chilton, D. P. Mills, Y.-Z. Zheng, *J. Am. Chem. Soc.* **2023**, *145*, 27993–28009.
[26] R. D. Shannon, *Acta Crystallogr. Sect. A* **1976**, *32*, 751–767.
[27] M. E. Fieser, M. R. Macdonald, B. T. Krull, J. E. Bates, J. W. Ziller, F. Furche, W. J. Evans, *J. Am. Chem. Soc.* **2015**, *137*, 369–382.
[28] M. C. Cassani, D. J. Duncalf, M. F. Lappert, *J. Am. Chem. Soc.* **1998**, *120*, 12958–12959.
[29] A. Falceto, D. Casanova, P. Alemany, S. Alvarez, *Chem. Eur. J.* **2014**, *20*, 14674–14689.
[30] F. H. Allen, O. Kennard, D. G. Watson, L. Brammer, A. G. Orpen, R. Taylor, *J. Chem. Soc. Perkin Trans. 2* **1987**, S1–S19.
[31] a) M. C. Cassani, Y. K. Gun'ko, P. B. Hitchcock, M. F. Lappert, *Chem. Commun.* **1996**, 1987–1988; b) M. C. Cassani, Y. K. Gun'ko, P. B. Hitchcock, M. F. Lappert, F. Laschi, *Organometallics* **1999**, *18*, 5539–5547.
[32] J. Mai, M. Morasch, D. Jędrzkiewicz, J. Langer, B. Rösch, S. Harder, *Angew. Chem. Int. Ed.* **2023**, *62*, e202212463.
[33] P. L. Arnold, S. M. Mansell, L. Maron, D. McKay, *Nat. Chem.* **2012**, *4*, 668–674.
[34] P. L. Arnold, A. Prescimone, J. H. Farnaby, S. M. Mansell, S. Parsons, N. Kaltsoyannis, *Angew. Chem.* **2015**, *127*, 6839–6843.
[35] T. Yanai, D. P. Tew, N. C. Handy, *Chem. Phys. Lett.* **2004**, *393*, 51–57.
[36] A. E. Reed, F. Weinhold, *J. Chem. Phys.* **1985**, *83*, 1736–1740.
[37] E. D. Glendening, C. R. Landis, F. Weinhold, *J. Comput. Chem.* **2013**, *34*, 1429–1437.
[38] C. A. Gould, J. Marbey, V. Vieru, D. A. Marchiori, R. David Britt, L. F. Chibotaru, S. Hill, J. R. Long, *Nat. Chem.* **2021**, *13*, 1001–1005.
[39] P. von R Schleyer, C. Maerker, A. Dransfeld, H. Jiao, N. J. R. van Eikema Hommes, *J. Am. Chem. Soc.* **1996**, *118*, 6317–6318.
[40] J. F. Corbey, D. H. Woen, C. T. Palumbo, M. E. Fieser, J. W. Ziller, F. Furche, W. J. Evans, *Organometallics* **2015**, *34*, 3909–3921.
[41] J. W. Lauher, R. Hoffmann, *J. Am. Chem. Soc.* **1976**, *98*, 1729–1742.
[42] R. Jena, F. Benner, F. Delano IV, D. Holmes, J. McCracken, S. Demir, A. L. Odom, *Chem. Sci.* **2023**, *14*, 4257–4264.
[43] M. T. Dumas, J. W. Ziller, W. J. Evans, *ACS Omega* **2019**, *4*, 398–402.
[44] G. R. Fulmer, A. J. M. Miller, N. H. Sherden, H. E. Gottlieb, A. Nudelman, B. M. Stoltz, J. E. Bercaw, K. I. Goldberg, *Organometallics* **2010**, *29*, 2176–2179.
[45] H. L. C. Feltham, S. Brooker, *Coord. Chem. Rev.* **2014**, *276*, 1–33.
[46] A. P. Orlova, J. D. Hilgar, M. G. Bernbeck, M. Gembicky, J. D. Rinehart, *J. Am. Chem. Soc.* **2022**, *144*, 11316–11325.
[47] M. G. Bernbeck, A. P. Orlova, J. D. Hilgar, M. Gembicky, M. Ozerov, J. D. Rinehart, *J. Am. Chem. Soc.* **2024**, *146*, 7243–7256.
[48] R. Sessoli, D. Gatteschi, A. Caneschi, M. A. Novak, *Nature* **1993**, *365*, 141–143.
[49] F.-S. Guo, B. M. Day, Y.-C. Chen, M.-L. Tong, A. Mansikkamäki, R. A. Layfield, *Science* **2018**, *362*, 1400–1403.
[50] C. A. P. Goodwin, F. Ortu, D. Reta, N. F. Chilton, D. P. Mills, *Nature* **2017**, *548*, 439–442.
[51] K. R. McClain, C. A. Gould, K. Chakarawet, S. J. Teat, T. J. Groshens, J. R. Long, B. G. Harvey, *Chem. Sci.* **2018**, *9*, 8492–8503.
[52] J. C. Vanjak, B. O. Wilkins, V. Vieru, N. S. Bhuvanesh, J. H. Reibenspies, C. D. Martin, L. F. Chibotaru, M. Nippe, *J. Am. Chem. Soc.* **2022**, *144*, 17743–17747.
[53] S. Demir, I.-R. Jeon, J. R. Long, T. D. Harris, *Coord. Chem. Rev.* **2015**, *289–290*, 149–176.
[54] J. D. Rinehart, M. Fang, W. J. Evans, J. R. Long, *J. Am. Chem. Soc.* **2011**, *133*, 14236–14239.
[55] S. Demir, M. I. Gonzalez, L. E. Darago, W. J. Evans, J. R. Long, *Nat. Commun.* **2017**, *8*, 2144.
[56] F. Benner, L. L. Droitte, O. Cador, B. L. Guennic, S. Demir, *Chem. Sci.* **2023**, *14*, 5577–5592.
[57] C. A. Gould, K. R. McClain, D. Reta, J. G. C. Kragskow, D. A. Marchiori, E. Lachman, E.-S. Choi, J. G. Analytis,

R. D. Britt, N. F. Chilton, B. G. Harvey, J. R. Long, *Science* **2022**, *375*, 198–202.
[58] C. T. Palumbo, L. E. Darago, M. T. Dumas, J. W. Ziller, J. R. Long, W. J. Evans, *Organometallics* **2018**, *37*, 3322–3331.
[59] D. Reta, N. F. Chilton, *Phys. Chem. Chem. Phys.* **2019**, *21*, 23567–23575.
[60] W. Huang, J. J. Le Roy, S. I. Khan, L. Ungur, M. Murugesu, P. L. Diaconescu, *Inorg. Chem.* **2015**, *54*, 2374–2382.
[61] Z. Lu, G. P. A. Yap, D. S. Richeson, *Organometallics* **2001**, *20*, 706–712.
[62] CrysAlisPro Software System **2020**.
[63] SCALE3 ABSPACK Empirical Absorption Correction, CrysAlis Pro - Software Package **2020**.
[64] G. Sheldrick, *Acta Crystallogr. Sect. A* **2015**, *71*, 3–8.
[65] G. Sheldrick, *Acta Crystallogr. Sect. C* **2015**, *71*, 3–8.
[66] O. V. Dolomanov, L. J. Bourhis, R. J. Gildea, J. A. K. Howard, H. Puschmann, *J. Appl. Crystallogr.* **2009**, *42*, 339–341.
[67] M. J. Frisch, G. W. Trucks, H. B. Schlegel, G. E. Scuseria, M. A. Robb, J. R. Cheeseman, G. Scalmani, V. Barone, G. A. Petersson, H. Nakatsuji, X. Li, M. Caricato, A. V. Marenich, J. Bloino, B. G. Janesko, R. Gomperts, B. Mennucci, H. P. Hratchian, J. V. Ortiz, A. F. Izmaylov, J. L. Sonnenberg, D. Williams-Young, F. Ding, F. Lipparini, F. Egidi, J. Goings, B. Peng, A. Petrone, T. Henderson, D. Ranasinghe, V. G. Zakrzewski, J. Gao, N. Rega, G. Zheng, W. Liang, M. Hada, M. Ehara, K. Toyota, R. Fukuda, J. Hasegawa, M. Ishida, T. Nakajima, Y. Honda, O. Kitao, H. Nakai, T. Vreven, K. Throssell, J. A. Montgomery Jr, J. E. Peralta, F. Ogliaro, M. J. Bearpark, J. J. Heyd, E. N. Brothers, K. N. Kudin, V. N. Staroverov, T. A. Keith, R. Kobayashi, J. Normand, K. Raghavachari, A. P. Rendell, J. C. Burant, S. S. Iyengar, J. Tomasi, M. Cossi, J. M. Millam, M. Klene, C. Adamo, R. Cammi, J. W. Ochterski, R. L. Martin, K. Morokuma, O. Farkas, J. B. Foresman, D. J. Fox, *Gaussian16 Revision B.01* **2016**.
[68] K. A. Peterson, D. Figgen, M. Dolg, H. Stoll, *J. Chem. Phys.* **2007**, *126*, 124101.
[69] A. D. Becke, *J. Chem. Phys.* **1993**, *98*, 5648–5652.
[70] Y. Zhao, D. G. Truhlar, *Theor. Chem. Acc.* **2008**, *120*, 215–241.
[71] C. Adamo, V. Barone, *J. Chem. Phys.* **1999**, *110*, 6158–6170.
[72] J. Tao, J. P. Perdew, V. N. Staroverov, G. E. Scuseria, *Phys. Rev. Lett.* **2003**, *91*, 146401.
[73] V. N. Staroverov, G. E. Scuseria, J. Tao, J. P. Perdew, *J. Chem. Phys.* **2003**, *119*, 12129–12137.
[74] F. Weigend, R. Ahlrichs, *Phys. Chem. Chem. Phys.* **2005**, *7*, 3297–3305.
[75] K. L. Schuchardt, B. T. Didier, T. Elsethagen, L. Sun, V. Gurumoorthi, J. Chase, J. Li, T. L. Windus, *J. Chem. Inf. Model.* **2007**, *47*, 1045–1052.
[76] B. P. Pritchard, D. Altarawy, B. Didier, T. D. Gibson, T. L. Windus, *J. Chem. Inf. Model.* **2019**, *59*, 4814–4820.
[77] D. Feller, *J. Comput. Chem.* **1996**, *17*, 1571–1586.
[78] S. Grimme, J. Antony, S. Ehrlich, H. Krieg, *J. Chem. Phys.* **2010**, *132*, 154104.
[79] D. G. A. Smith, L. A. Burns, K. Patkowski, C. D. Sherrill, *J. Phys. Chem. Lett.* **2016**, *7*, 2197–2203.
[80] V. Barone, M. Cossi, *J. Phys. Chem. A* **1998**, *102*, 1995–2001.
[81] M. Cossi, N. Rega, G. Scalmani, V. Barone, *J. Comput. Chem.* **2003**, *24*, 669–681.
[82] C. M. Kotyk, M. E. Fieser, C. T. Palumbo, J. W. Ziller, L. E. Darago, J. R. Long, F. Furche, W. J. Evans, *Chem. Sci.* **2015**, *6*, 7267–7273.
[83] M. Carrasco, N. Curado, C. Maya, R. Peloso, A. Rodríguez, E. Ruiz, S. Alvarez, E. Carmona, *Angew. Chem. Int. Ed.* **2013**, *52*, 3227–3231.
[84] W. H. Monillas, G. P. A. Yap, K. H. Theopold, *Angew. Chem. Int. Ed.* **2007**, *46*, 6692–6694.
[85] Y.-C. Tsai, P.-Y. Wang, S.-A. Chen, J.-M. Chen, *J. Am. Chem. Soc.* **2007**, *129*, 8066–8067.
[86] Y.-C. Tsai, P.-Y. Wang, K.-M. Lin, S.-A. Chen, J.-M. Chen, *Chem. Commun.* **2007**, 205–207.
[87] R. P. Kelly, D. Toniolo, F. F. Tirani, L. Maron, M. Mazzanti, *Chem. Commun.* **2018**, *54*, 10268–10271.
[88] D. Patel, F. Moro, J. McMaster, W. Lewis, A. J. Blake, S. T. Liddle, *Angew. Chem. Int. Ed.* **2011**, *50*, 10388–10392.
[89] D. P. Mills, F. Moro, J. McMaster, J. Van Slageren, W. Lewis, A. J. Blake, S. T. Liddle, *Nat. Chem.* **2011**, *3*, 454–460.
[90] S. Krieck, H. Görls, L. Yu, M. Reiher, M. Westerhausen, *J. Am. Chem. Soc.* **2009**, *131*, 2977–2985.
[91] A. J. Wooles, W. Lewis, A. J. Blake, S. T. Liddle, *Organometallics* **2013**, *32*, 5058–5070.
[92] V. Mougel, C. Camp, J. Pécaut, C. Copéret, L. Maron, C. E. Kefalidis, M. Mazzanti, *Angew. Chem. Int. Ed.* **2012**, *51*, 12280–12284.
[93] P. L. Diaconescu, C. C. Cummins, *Inorg. Chem.* **2012**, *51*, 2902–2916.
[94] A. A. Danopoulos, P. Braunstein, K. Y. Monakhov, J. van Leusen, P. Kögerler, M. Clémancey, J.-M. Latour, A. Benayad, M. Tromp, E. Rezabal, G. Frison, *Dalton Trans.* **2017**, *46*, 1163–1171.
[95] K. Angermund, K. H. Claus, R. Goddard, C. Krüger, *Angew. Chem. Int. Ed. Engl.* **1985**, *24*, 237–247.
[96] J. L. Priego, L. H. Doerrer, L. H. Rees, M. L. H. Green, *Chem. Commun.* **2000**, *0*, 779–780.
[97] W. Frank, V. Reiland, G. J. Reiß, *Angew. Chem. Int. Ed.* **1998**, *37*, 2983–2985.
[98] Y. Luo, Y. Yao, Q. Shen, K. Yu, L. Weng, *Eur. J. Inorg. Chem.* **2003**, 318–323.
[99] C. Camp, V. Mougel, J. Pécaut, L. Maron, M. Mazzanti, *Chem. Eur. J.* **2013**, *19*, 17528–17540.
[100] F. A. Cotton, P. A. Kibala, W. A. Wojtczak, *J. Am. Chem. Soc.* **1991**, *113*, 1462–1463.
[101] D. E. DeRosha, B. Q. Mercado, G. Lukat-Rodgers, K. R. Rodgers, P. L. Holland, *Angew. Chem. Int. Ed.* **2017**, *56*, 3211–3215.
[102] P. L. Diaconescu, P. L. Arnold, T. A. Baker, D. J. Mindiola, C. C. Cummins, *J. Am. Chem. Soc.* **2000**, *122*, 6108–6109.
[103] W. J. Evans, S. A. Kozimor, J. W. Ziller, N. Kaltsoyannis, *J. Am. Chem. Soc.* **2004**, *126*, 14533–14547.
[104] W. J. Evans, C. A. Traina, J. W. Ziller, *J. Am. Chem. Soc.* **2009**, *131*, 17473–17481.
[105] T. L. Gianetti, G. Nocton, S. G. Minasian, N. C. Tomson, A. L. D. Kilcoyne, S. A. Kozimor, D. K. Shuh, T. Tyliszczak, R. G. Bergman, J. Arnold, *J. Am. Chem. Soc.* **2013**, *135*, 3224–3236.
[106] T. L. Gianetti, G. Nocton, S. G. Minasian, N. Kaltsoyannis, A. L. D. Kilcoyne, S. A. Kozimor, D. K. Shuh, T. Tyliszczak, R. G. Bergman, J. Arnold, *Chem. Sci.* **2015**, *6*, 993–1003.
[107] R. Gyepes, J. Pinkas, I. Císařová, J. Kubišta, M. Horáček, K. Mach, *RSC Adv.* **2016**, *6*, 94149–94159.
[108] Y. S. Huang, G. T. Huang, Y. L. Liu, J. S. K. Yu, Y. C. Tsai, *Angew. Chem. Int. Ed.* **2017**, *56*, 15427–15431.
[109] A. F. R. Kilpatrick, J. C. Green, Z. R. Turner, J. C. Buffet, D. O'Hare, *Chem. Commun.* **2017**, *53*, 12048–12051.
[110] M. J. Monreal, S. I. Khan, J. L. Kiplinger, P. L. Diaconescu, *Chem. Commun.* **2011**, *47*, 9119–9121.
[111] C. Ni, B. D. Ellis, J. C. Fettinger, G. J. Long, P. P. Power, *Chem. Commun.* **2008**, 1014–1016.

Manuscript received: September 7, 2024
Accepted manuscript online: October 14, 2024
Version of record online: December 5, 2024